Dalton Transactions

PAPER

View Article Online
View Journal | View Issue

Cite this: *Dalton Trans.*, 2016, **45**, 18719

A lysosome targetable luminescent bioprobe based on a europium β-diketonate complex for cellular imaging applications†

T. M. George,[a,b] Mahesh S. Krishna[c] and M. L. P. Reddy*[a,b]

Received 4th October 2016,
Accepted 31st October 2016

DOI: 10.1039/c6dt03833f

www.rsc.org/dalton

Herein, we report a novel lysosome targetable luminescent bioprobe derived from a europium coordination compound, namely Eu(pfphOCH$_3$IN)$_3$(DDXPO) **4** [where HpfphOCH$_3$IN = 4,4,5,5,5-pentafluoro-3-hydroxy-1-(1-(4-methoxyphenyl)-1*H*-indol-3-yl)pent-2-en-1-one and DDXPO = 4,5-bis(diphenylphosphino)-9,9-dimethylxanthene oxide]. Notably, the newly designed europium complex exhibits significant quantum yield ($\Phi_{overall}$ = 25 ± 3%) and $^5D_0$ excited state lifetime (τ = 398 ± 3 μs) values under physiological pH (7.2) conditions when excited at 405 nm. Hence the developed europium complex has been evaluated for live cell imaging applications using mouse pre-adipocyte cell lines (3T3L1). Colocalization studies of the designed bio-probe with commercial Lysosome-GFP in 3T3L1 cells demonstrated the specific localization of the probe in the lysosome with a high colocalization coefficient (*A* = 0.83). Most importantly, the developed bioprobe exhibits good cell permeability, photostability and non-cytotoxicity.

Introduction

In recent years, luminescent lanthanide bioprobes have emerged as viable alternatives to existing organic fluorescent probes due to their unique photophysical properties and several distinct advantages, such as less sensitive nature to photobleaching, long-lived excited state lifetimes and large Stokes' shifts upon ligand excitation.[1] The large Stokes' shifts benefit the avoidance of self-absorption of the ligand and reduce the background signals. The f–f transitions are formally forbidden by the spin and Laporte rule and hence feature long excited-state lifetimes in the milli to microsecond range. The long decay times offer an immense advantage for the time-gated detection of biological samples, wherein interfering short-lived autofluorescence and scattering are suppressed. Due to shielding of the 5s and 5p orbitals in lanthanides, the 4f orbitals do not directly participate in chemical bonding. Thus the emission wavelengths of lanthanides are minimally perturbed by the surrounding matrix and ligand field, resulting in sharp and line-like emission bands.[2] These properties confer luminescent Ln^{3+} complexes for time-gated or time-resolved live-cell or *in vivo* imaging. Such an approach enhances signal-to-noise ratios through the elimination of interferences from scattering and short-lived autofluorescence of biological species.[3,4] Finally, the antenna effect has another advantage, while the excitation of the ligand has been performed in the UV to blue spectral regions; emission is noted in the visible or NIR domains, and the pseudo-Stokes shift is large, decreasing the need for efficient filtering between the excitation and emission channels.[5] As a consequence, a large number of luminescent bioprobes have been developed for cellular imaging applications and these data are covered in pioneering review articles.[1,3,6] However, a major limitation of the existing lanthanide probes is that the excitation window is limited to the UV region.[7] Another problem with the currently available lanthanide luminescent probes is photobleaching, especially when the sample is exposed to continuous intense excitation for monitoring the biological processes, typically the luminescence imaging of cellular and histochemical processes.[8] Thus it is of paramount importance to extend the excitation window towards the visible region to minimize the effects of excitation phototoxicity on the biological samples.

Nevertheless, a major challenge in live-cell imaging is the creation of selective stain-compounds that enter cells and localize preferentially to a particular organelle without perturbing cell homeostasis.[1b] Numerous luminescent lanthanide

[a]*AcSIR-Academy of Scientific & Innovative Research, CSIR-NIIST Campus, Thiruvananthapuram, India*
[b]*Materials Science and Technology Division, National Institute for Interdisciplinary Science and Technology (NIIST), Council of Scientific and Industrial Research (CSIR), Thiruvananthapuram-695 019, India. E-mail: mlpreddy55@gmail.com*
[c]*Cardiovascular Diseases and Diabetes Biology Lab, Rajiv Gandhi Centre for Biotechnology, Thiruvananthapuram, India*

†Electronic supplementary information (ESI) available. See DOI: 10.1039/c6dt03833f

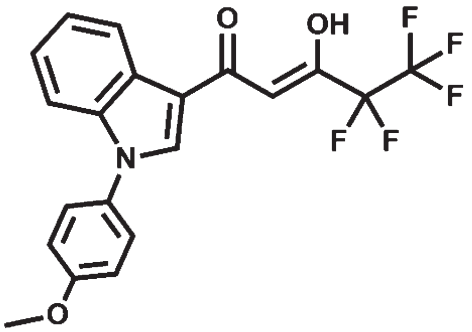

Fig. 1 Structure of the ligand HpfphOCH$_3$IN.

coordination compounds based on cryptates,[9] helicates,[10] polyaminocarboxylates,[11] aminophosphinates,[12] β-diketonates[13] and notably based on 9-N_3 or 12-N_4 ligand frameworks[6a,14] have been developed that are tackled to meet a set of stringent requirements for use as cellular stains.[15] To utilize the luminescent europium complex for live cell imaging applications, it must possess certain biological properties. Importantly, the luminescent complex must readily cross the cell membrane and localize in a region of interest within the cell. These important biological properties have led to recent efforts by many investigators to characterize the subcellular behaviour of a large number of sensitized lanthanide complexes.[1h,13b,c] Typically, a pH sensor might be best localized in lysosomes, in which acidity can signify endosome age or health.[1h,16] Recently, cyclometalated iridium(III) complexes containing β-carboline (a kind of biologically active indole alkaloid) as ligands have been reported as pH responsive tumor/lysosome-targeted PDT agents.[17] The use of terpyridine as an ancillary ligand in europium β-diketonate complexes exhibits selectivity towards the mitochondria of living cells.[13b,c] On the basis of wide existence, and the important physiological activities of indole derivatives, especially its lysosome specificity in live cell imaging, in the current study, a new β-diketone ligand namely 4,4,5,5,5-pentafluoro-3-hydroxy-1-(1-(4-methoxyphenyl)-1*H*-indol-3-yl)pent-2-en-1-one (Fig. 1) has been synthesized and utilized for the development of a Eu^{3+} ternary complex in the presence of an ancillary ligand (DDXPO). The developed coordination compound has been characterized by various spectroscopic techniques and its photophysical properties were evaluated under biologically relevant pH conditions with a view to develop a bioprobe for cellular imaging applications.

Experimental

Materials and characterization

The chemicals were acquired from commercial sources and used as purchased: europium(III) nitrate hexahydrate, 99.99% (Alfa Aesar); gadolinium(III) nitrate hexahydrate, 99.999% (Sigma Aldrich); lanthanum(III) nitrate hexahydrate, 99.99% (Sigma Aldrich); sodium hydride 60% dispersion in mineral oil (Sigma Aldrich); ethyl pentafluoropropionate, 98% (Sigma Aldrich); 4,5-bis(diphenylphosphino)-9,9-dimethylxanthene, 97% (Sigma Aldrich); 3-acetylindole, 98% (Alfa Aesar); 4-methoxyphenylboronic acid, 98% (Alfa Aesar); diisopropylethylamine, 99% (Alfa Aesar) and copper(II) acetate, 97% (Sigma Aldrich). All the other chemical materials purchased were of analytical reagent grade and used as supplied.

Elemental analyses were performed on an Elementar-vario MICRO cube elemental analyzer. The FT-IR spectral data were recorded using KBr pellets on a Perkin-Elmer Spectrum two FT-IR spectrometer. The NMR data of the ligands as well as designed lanthanide complexes were recorded using a Bruker 500 MHz NMR spectrometer [^{1}H NMR (500 MHz); ^{13}C NMR (125.7 MHz) and ^{31}P NMR (202.44 MHz)] in chloroform-d solution. The chemical shift values are expressed in parts per million relative to tetramethylsilane ($SiMe_4$) for ^{1}H NMR and ^{13}C NMR spectra, and with respect to 85% phosphoric acid for ^{31}P NMR spectra. Electrospray ionization (ESI) mass spectra were acquired by using a Thermo Scientific Exactive Benchtop LC/MS Orbitrap mass spectrometer. The absorption spectra of the ligand and the corresponding Eu^{3+}complex were recorded with a UV-vis spectrophotometer (Shimadzu, UV-2450). The solution state photoluminescence (PL) spectrum was recorded on a Spex-Fluorolog FL22 spectrofluorimeter equipped with a double grating 0.22 m Spex 1680 monochromator and a 450W Xe lamp as the excitation source. Lifetime measurement was recorded at room temperature using a Spex 1040D phosphorimeter. The overall quantum yield ($\Phi_{overall}$) was studied in a buffer solution of pH 7.2 (Hanks' Balanced Salt Solution, HBSS) at 298 K using eqn (1) and is measured relative to a quinine sulfate in 1 N H_2SO_4 solution (Φ_{ref} = 54.6%),[18]

$$\Phi_{overall} = \frac{n^2 A_{ref} I}{n_{ref}{}^2 A I_{ref}} \Phi_{ref} \quad (1)$$

where n, A, and I denote the refractive index of the solvent, the absorbance at the excitation wavelength and the area of the emission spectrum, respectively, and Φ_{ref} represents the quantum yield of the standard quinine sulfate solution. The subscript ref denotes the reference, and the absence of a subscript implies an unknown sample. The refractive index is assumed to be equivalent to that of the pure solvent: 1.33 for water at room temperature. All data reported are averages of at least three independent measurements.[13b]

Synthetic procedures

Synthesis of 1-(1-(4-methoxyphenyl)-1*H*-indol-3-yl)ethanone. A mixture of 3-acetylindole (1.0 mmol), 4-methoxyphenylboronic acid (2.5 mmol), anhydrous copper(II) acetate (2.5 mmol) and diisopropylethylamine (99%, 2.5 mmol) in 2 mL dry dichloromethane (DCM) was taken in a sealed flask (25 mL) and stirred at room temperature for 24 h. From the resultant reaction mixture, DCM was removed under reduced pressure. Then 10 mL of water and 10 mL of chloroform were added. The corresponding aqueous layer was extracted with chloroform (2 × 10 mL). The concentrated organic layer was purified by column chromatography on silica gel using ethyl acetate and

hexane (2 : 98) as the eluent. Yield: 80%. ^{1}H NMR ($CDCl_3$, 500 MHz) δ (ppm): 8.44 (d, 1H, J = 8.0 Hz), 7.88 (s, 1H), 7.35 (m, 5H), 7.06 (d, 2H, J = 9.0 Hz), 3.89 (s, 3H), 2.57 (s, 3H). ^{13}C NMR (125.7 MHz, $CDCl_3$) δ (ppm): 193.31, 159.29, 137.53, 135.01, 131.21, 126.46, 126.30, 123.79, 122.96, 122.67, 118.29, 114.97, 110.76, 55.67, 27.71. m/z = 266.11 $(M + H)^+$.

Synthesis of the ligand 4,4,5,5,5-pentafluoro-3-hydroxy-1-(1-(4-methoxyphenyl)-1*H*-indol-3-yl)pent-2-en-1-one. ($HpfphOCH_3IN$). A modified Claisen condensation procedure is used for the synthesis of a new β-diketonate ligand as described in Scheme 1. 1-(1-(4-Methoxyphenyl)-1*H*-indol-3-yl)ethanone (1.0 mmol) and ethyl pentafluoropropionate (1.0 mmol) were added to 15 mL of dried tetrahydrofuran (THF) and stirred for 10 min at 0 °C under a nitrogen atmosphere. Sodium hydride (2.0 mmol) was added to the above reaction mixture and stirred for 20 min followed by stirring at 60 °C for 24 h. After cooling the reaction mixture to room temperature, 2 M HCl (25 mL) was added and then the suspension was extracted thrice with dichloromethane (3 × 20 mL). The organic layer was dried over Na_2SO_4, and the solvent was evaporated. The obtained crude product is then purified by silica gel column chromatography using the solvent mixture of ethyl acetate and hexane (1 : 99) as the eluent to obtain the product. Yield: 85%. Elemental analysis (%): calculated for $C_{20}H_{14}F_5NO_3$ (412.09): C 58.43, H 3.43, N 3.41; Found: C 58.54, H 3.36, N 3.48. ^{1}H NMR ($CDCl_3$, 500 MHz) δ (ppm): 15.96 (broad, enol–OH), 8.30 (d, 1H, J = 7.5 Hz), 7.42–7.32 (m, 5H), 7.08 (s, 2H, J = 9.0 Hz), 6.48 (s, 1H), 3.90 (s, 3H). ^{13}C NMR (125.7 MHz, in $CDCl_3$) δ (ppm): 184.85, 172.77, 159.73, 138.07, 134.90, 130.52, 126.47, 125.75, 124.46, 123.68, 122.34, 119.29, 115.09, 113.50, 111.53, 94.53, 55.70. FT-IR (KBr) ν_{max} (cm^{-1}): 3425, 2944, 1616, 15151460, 1324, 1254, 1209, 1028, 832 741. m/z = 412.09 $(M + H)^+$.

Synthesis of $Ln(pfphOCH_3IN)_3(H_2O)_2$ [Ln = Eu^{3+} (1), Gd^{3+} (2), and La^{3+} (3)] complexes. To a methanolic solution of β-diketonate ligand ($HpfphOCH_3IN$, 3.0 mmol), NaOH (3.0 mmol) in water was added and stirred for 5 min. To this solution, $Ln(NO_3)_3{\cdot}6(H_2O)$ (where Ln = Eu^{3+}, Gd^{3+}, La^{3+}) (1.0 mmol) in 2 mL methanol was added dropwise and it was further stirred for 24 h at room temperature. The precipitate formed after the addition of water was filtered off and dried. The solid product was isolated by recrystallization from chloroform solution and used for analysis and photophysical properties. Attempts to grow single crystals of complexes were unsuccessful. The synthesis procedure is detailed in Scheme 2.

$Eu(pfphOCH_3IN)_3(H_2O)_2$ (1). Elemental analysis (%): calculated for $C_{60}H_{43}F_{15}N_3O_{11}Eu$ (1418.94): C 51.03, H 3.17, N 2.93; Found: C 51.21, H 3.25, N 2.91. IR (KBr) ν_{max} (cm^{-1}): 3425, 2916, 1598, 1518, 1453, 1333, 1249, 1203, 1036, 833, 740. m/z = 1384.17 $[Eu(pfphOCH_3IN)_3]^+$.

$Gd(pfphOCH_3IN)_3(H_2O)_2$ (2). Elemental analysis (%): calculated for $C_{60}H_{43}F_{15}N_3O_{11}Gd$ (1424.22): C 50.60, H 3.04, N 2.95; Found: C 50.68, H 3.23, N 2.98. IR (KBr) ν_{max} (cm^{-1}): 3424, 2925, 1601, 1516, 1453, 1360, 1213, 1035, 834, 745. m/z = 1389.17 $[Gd(pfphOCH_3IN)_3+H]^+$.

$La(pfphOCH_3IN)_3(H_2O)_2$ (3). Elemental analysis (%): calculated for $C_{60}H_{43}F_{15}N_3O_{11}La$ (1405.17): C 51.26, H 3.08, N 2.99; Found: C 51.37, H 3.05, N 3.11. ^{1}H NMR ($CDCl_3$, 500 MHz) δ (ppm): 8.38 (d, 3H), 7.79 (s, 3H), 7.36 (s, 1H), 7.26 (m, 15H) 7.05–6.97 (m, 5H), 6.35 (s, 3H), 3.86 (s, 9H). IR (KBr) ν_{max} (cm^{-1}): 3428, 2926, 1599, 1460, 1213, 1182, 1036, 907, 750. m/z = 1411.29 $[La(pfphOCH_3IN)_3(H_2O)+Na]^+$.

Synthesis of Ln^{3+} complexes $Ln(pfphOCH_3IN)_3(DDXPO)$ [Ln = Eu^{3+} (4) and La^{3+} (5)]. Ternary Ln^{3+} complexes were synthesized by stirring equimolar quantities of the corresponding europium or lanthanum binary complexes and DDXPO in $CHCl_3$ solution for 12 h at 70 °C. The products were isolated by solvent evaporation and purified by recrystallization from dichloromethane and hexane. The procedure is described in Scheme 3.

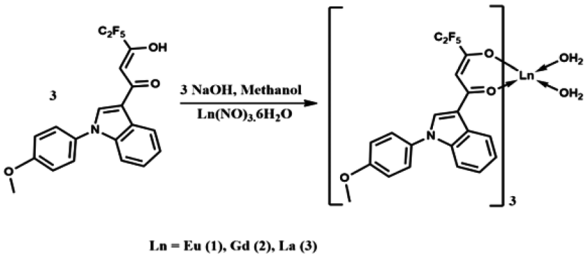

Scheme 2 Synthesis of the Ln^{3+} (Ln = Eu (1), Gd (2) and La (3)) complexes.

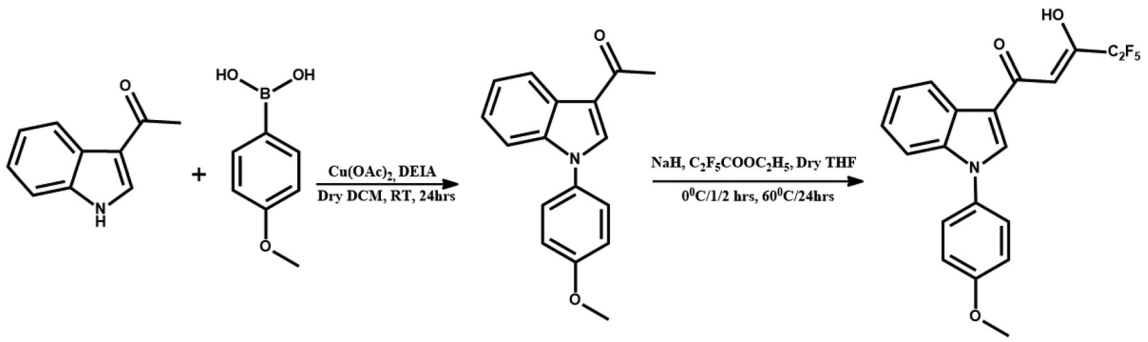

Scheme 1 Synthetic procedure for the ligand $HpfphOCH_3IN$.

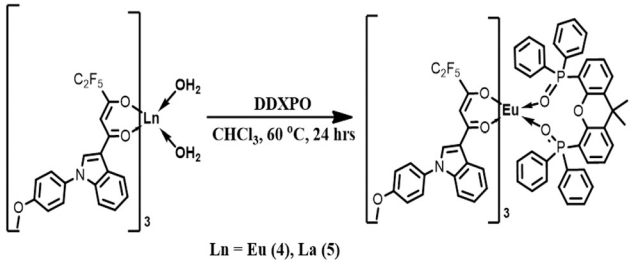

Scheme 3 Synthetic procedure for the Ln^{3+} complexes **4** and **5**.

Eu(pfphOCH$_3$IN)$_3$(DDXPO) (4). Elemental analysis (%): calculated for $C_{99}H_{71}O_{12}F_{15}N_3P_2Eu$ (1993.52): C 59.65, H 3.59, N 2.11; Found: C 59.73, H 3.62, N 2.26. IR (KBr) ν_{max} (cm^{-1}): 3028, 1601, 1514, 1457, 1405, 1360, 1180, 1216, 1037, 904, 745. *m*/*z* = 1583.26 [Eu(pfphOCH$_3$IN)$_2$(DDXPO)]$^+$. ^{31}P NMR ($CDCl_3$, 202.44 MHz) δ (ppm): −80.86.

La(pfphOCH$_3$IN)$_3$(DDXPO) (5). Elemental analysis (%): calculated for $C_{99}H_{71}O_{12}F_{15}N_3P_2La$(1979.33): C 60.04, H 3.61, N 2.12; Found: C 60.22, H 3.57, N 2.35. ^{1}H NMR ($CDCl_3$, 500 MHz) δ (ppm): 8.57 (d, 3H), 7.57 (s, 3H), 7.41 (m, 8H), 7.36–7.35 (m, 4H), 7.29–7.23 (m, 9H), 7.10–7.07 (m, 4H), 7.04–7.01 (m, 3H), 6.97–6.99 (m, 6H), 6.86 (s, 7H), 6.71 (t, 3H),6.04 (s, 3H), 6.53 (m, 2H), 6.32 (s, 2H), 3.87 (s, 9H), 1.61 (s, 6H). IR (KBr) ν_{max} (cm^{-1}): 3064, 1600, 1515, 1452, 1325, 1182, 1098, 1036, 745. *m*/*z* = 1570.18 [La(pfphOCH$_3$IN)$_2$(DDXPO)]$^+$. ^{31}P NMR ($CDCl_3$, 202.44 MHz) δ (ppm): 31.85.

Sample preparation for biological studies

Complex **4** was dissolved in DMSO at a concentration of 100 mg mL^{-1}. Sub stocks were prepared at desired concentrations in Dulbecco's Minimal Essential Medium (DMEM, Sigma-Aldrich) so that the final concentration of DMSO in cell culture should be less than 0.01%. All the biological studies using complex **4** were performed at a pH of 7.2 which is a critical factor for regular cellular function.

Cytotoxicity and cell imaging studies

Cytotoxicity measurement of complex **4** on 3T3L1 cell lines (mouse pre-adipocyte cell lines, National Centre for Cell Science, Pune, India) was performed. Dulbecco's modified Eagle's medium (DMEM, Sigma-Aldrich), fetal bovine serum (FBS, Sigma-Aldrich), antibiotic (1% penicillin/streptomycin, Sigma-Aldrich) and MTT (3-[4,5-dimethylthiazol-2-yl]-2,5-diphenyltetrazolium bromide, Sigma-Aldrich) are the chemicals and reagents used.

Cell culture

The cells were cultured in DMEM supplemented with 10% fetal bovine serum (FBS) and an antibiotic (1% penicillin/streptomycin) in 5% CO_2 at 37 °C and 99% humidity. The cells from exponentially growing cultures were used for the experiments. The growth medium was changed every other day until the time of use of the cells.

MTT assay for cytotoxicity studies

The cytotoxicity of complex **4** was analysed by the MTT assay as per the reference protocol (Wilson, 2000).[19] Briefly, 1×10^4 per mL cells were seeded at the log phase in 96 well plates and incubated for 24 h. Growth media were removed and fresh media with complex **4** at different concentrations (0.05, 5, 25, 50 and 125 μM) and DMSO as the control were incubated for 16 h. Next day, the sample containing media was removed and the cells were incubated with MTT (50 μg mL^{-1}) for 3–4 h. The crystals developed were solubilized by shaking in DMSO for 2 h and the absorbance was measured at 570 nm using a UV-Vis. spectrophotometer (UV-1700, Shimadzu, Japan). The percentage of cell viability was calculated and plotted against the concentration.

Fluorescence imaging and co-localization studies of Eu(pfphOCH$_3$IN)$_3$(DDXPO) with confocal microscopy

The cells were seeded (1×10^4 per well) in a 96 well black walled bio-imaging plate (BD Bioscience, USA) and incubated to approximately 70% confluence. The growth media were replaced with complex **4** containing media at 0.5, 5, 25 and 50 μM concentration and incubated for 24 h. The fluorescence of the compound was imaged using a confocal microscope (SP8 WLL, Leica, Gmbh) after three times wash using Hanks' Balanced Salt Solution (HBSS). The fluorescence of complex **4** at different time intervals was also analyzed as part of standardization. Co-localization studies of complex **4** were carried out after lysosome and mitochondrial staining using CellLight® Lysosome-GFP, BacMam 2.0 and CellLight mito-GFP, BacMam 2.0, respectively (Thermo Fisher Scientific, USA). Briefly, the cells after reaching the 70% confluent stage were incubated with a viral particle load of 1×10^8 mL^{-1} calculating an approximate value of 30 particles per cell (PPC) as per the manufacturer's instruction. The cells were incubated for 16–18 hours in the presence of CellLight solution. The images were obtained from Lysosome-GFP/mitochondrial-GFP using an excitation source of 488 nm and monitoring the emission wavelength at 520 nm. These images were then merged/overlaid on the images acquired using the excitation signal of 405 nm and the emission wavelength of 612 nm.

Results and discussion

Synthesis and characterization of HpfphOCH$_3$IN ligand and Ln^{3+} complexes 1–5

The β-diketonate ligand (HpfphOCH$_3$IN) was synthesized with an overall yield of 85% adapting the protocol as summarized in Scheme 1. The detailed characterization of the designed ligand has been carried out by ^{1}H NMR, ^{13}C NMR, FT-IR and electron spray ionization mass spectroscopic (ESI-MS) methods (Fig. S1–S4 in the ESI†) as well as by elemental analysis. The singlet peak observed in the ^{1}H NMR spectrum of the ligand at about 6.48 ppm (δ) is assigned to the methine proton. The active H^{enol} proton that can be observed at

15.96 ppm (δ) reveals that the β-diketonate ligand exists as an enol form in $CDCl_3$ solution. The other signals noted in the range of 7.07–8.30 ppm (δ) are attributed to the aromatic protons of the ligand. The ancillary ligand 4,5-bis(diphenylphosphino)-9,9-dimethylxanthene oxide (DDXPO) was prepared according to the literature procedure.[7d] The synthesis procedures for Ln^{3+} (Eu^{3+}, Gd^{3+} and La^{3+}) complexes are outlined in Schemes 2 and 3. The isolated lanthanide complexes were characterized by FT-IR, mass spectroscopy (ESI-MS) and elemental analyses. The elemental analyses and ESI-MS studies (Fig. S5–S7 in the ESI†) of Ln^{3+} complexes (**1–3**) indicate that the central Ln^{3+} ion is coordinated to three β-diketonate ligands. On the other hand, in the ternary Ln^{3+} complexes (**4** and **5**), one molecule of the bidentate oxygen donor, DDXPO, is also present in the coordination sphere of the metal ion (Fig. S8 and S9 in the ESI†). The IR carbonyl stretching frequency of the ligand $HpfphOCH_3IN$ (1616 cm^{-1}) is shifted to lower wavenumbers in **1–5** (1598 cm^{-1} for **1**; 1601 cm^{-1} for **2**; 1599 cm^{-1} for **3**; 1601 cm^{-1} for **4**; 1600 cm^{-1} for **5**), thus indicating the coordination of the carbonyl oxygen to the Ln^{3+} ion. In addition, the ($\nu_{P=O}$) stretching frequency of DDXPO (1190 cm^{-1}) has been shifted to lower wavenumbers in complex **4** (1180 cm^{-1}) and complex **5** (1182 cm^{-1}) which confirms the participation of the phosphoryl oxygen of DDXPO in the complex formation with Ln^{3+} ions (Fig. S10–S14 in the ESI†). This behaviour is further confirmed from the ^{31}P NMR spectral data (30.97 ppm in the DDXPO; −80.86 ppm in complex **4** shown in Fig. S15 in the ESI†).

In order to gain more information about the coordination behaviour of the europium complexes, in the present study the corresponding lanthanum complexes have been isolated and characterized by various spectral techniques (the pertinent data are given in the Experimental section). The ^1H NMR spectrum of $La(pfphOCH_3IN)_3(H_2O)_2$ is in accordance with the presence of three β-diketonate moieties coordinated to the central lanthanide ion (Fig. S16 in the ESI†). The ^1H NMR signal for the methine proton (–CH) of $HpfphOCH_3IN$ resonates at 6.35 ppm (δ) and the aromatic protons resonates in the range 8.39 to 6.97 ppm (δ). The observed upfield shift in the β-diketonate resonances, in the complex, reveals the coordination of $HpfphOCH_3IN$ ligands with the Ln^{3+} ion. The proton signals of the chelated water molecule with the Ln^{3+} ion can be seen at 1.88 ppm (δ). In the ternary lanthanum complex, $La(pfphOCH_3IN)_3(DDXPO)$, the methine proton appears at 6.05 ppm (δ). The signals due to the aromatic protons of the β-diketonate ligand ($HpfphOCH_3IN$) and DDXPO moiety were observed in the range 8.58 to 6.30 ppm (δ) (Fig. S17 in the ESI†). The proton signals that appeared in the ternary lanthanum complex indicate the existence of three $HpfphOCH_3IN$ units and one DDXPO moiety in the coordinated complex. Moreover, no signals for the coordinated water molecule are noted in the $La(pfphOCH_3IN)_3(DDXPO)$, which substantiates the replacement of coordinated water molecules by the chelating ligand in complex **5**.

The absorption spectra of the ligand and the Eu^{3+} complex

The absorption spectra of the ligand $HpfphOCH_3IN$ and the corresponding Eu^{3+} complex were investigated in aqueous media buffered to physiological pH 7.2 [% DMSO: % HBSS = 0.01: 99.99; $c = 2.5 \times 10^{-5}$ M] at 298 K (Fig. 2). The maximum absorption bands are observed at 435 nm for the β-diketonate ligand and at around 393 nm for the europium complex, which is attributed to the singlet–singlet n–π* enolic transition assigned to the β-diketonate moiety. Furthermore, the higher energy absorption band detected in the range of 280–300 nm can be ascribed to the $^1\pi$–π* transition of the aromatic moiety of the β-diketonate ligand. In comparison with the absorption maximum of the ligand, the absorption maximum of the complex is dramatically blue-shifted by about 42 nm, which may be due to the perturbation induced by the coordination of the Eu^{3+} ion. However, the spectral pattern of the complex is similar to that of the free ligand, suggesting that the coordination of the Eu^{3+} ion has no significant influence on the $^1\pi$–π* state energy. The determined molar absorption coefficient value of the Eu^{3+} complex at 393 nm, 3.58×10^4 L mol^{-1} cm^{-1}, is about three times higher than that of the ligand (393 nm, 1.26×10^4 L mol^{-1} cm^{-1}), indicating the presence of three β-diketonate ligands in the corresponding complex. The high molar absorption coefficient value noted in the case of the ligand clearly illustrates the good light absorption ability of the newly developed ligand.[20]

Photophysical properties

To evaluate the triplet energy (T_1) of the newly developed β-diketonate ligand, the low-temperature phosphorescence spectrum of the corresponding gadolinium complex was recorded and the results are shown in Fig. 3. In this work gadolinium chelate was used to estimate the triplet energy level of the ligand due to the following reasons: (i) strong spin-orbital coupling or the heavy atom effect of the Gd^{3+} ion increases the probability of intersystem crossing from the singlet to triplet excited state, and (ii) the energy level of the Gd^{3+} ion is too high to accept the energy from the triplet state of the antenna chromophore ligand, so that only ligand-based emission can be observed. As a consequence the triplet energy

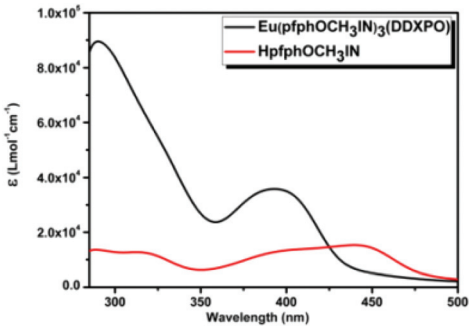

Fig. 2 UV-vis absorption spectra of the ligand $HpfphOCH_3IN$ and complex **4** in a buffer solution of pH 7.2 [% DMSO : % HBSS = 0.01 : 99.99; $c = 2.5 \times 10^{-5}$ M].

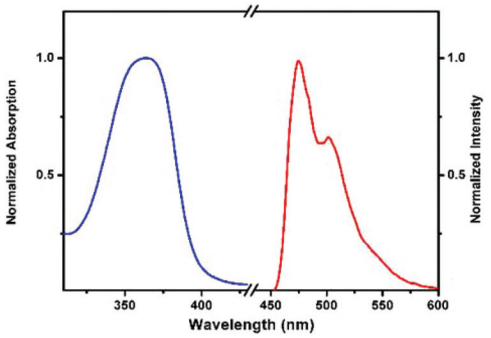

Fig. 3 UV-vis absorption spectrum at 298 K (left) and 77 K phosphorescence spectrum (right) of complex **2** in THF.

level of the ligand can be estimated from the lower emission edge of the phosphorescence spectrum.[5,21] The singlet energy level (S_1) of the ligand was determined from the upper absorption edge of the electronic spectrum of the Gd^{3+} complex (Fig. 3).[5] Thus the singlet and triplet energy levels of the β-diketonate ligand are found to be 25 000 cm^{-1} (400 nm) and 21 881 cm^{-1} (457 nm), respectively. As per the Dexter theory, the intramolecular energy transfer from the triplet state (T_1) of the ligand to the emitting resonance level of the lanthanide ion has a significant influence on europium luminescence. It is interesting to note that the energy gap between the triplet state of the newly designed β-diketonate ligand and the $^5D_0$ excited state of the Eu^{3+} ion (17 250 cm^{-1}) is found to be ΔE = 4631 cm^{-1}, which is considered to be an ideal situation for sensitization of Eu^{3+} luminescence.[5] The energy gap between the S_1 and T_1 states of $HpfphOCH_3IN$, $\Delta E = (S_1–T_1)$ 3119 cm^{-1}, which is again considered as optimum for intersystem crossing in visible-light excited europium complexes.[5k]

The excitation and emission profiles of the developed europium complex recorded in a buffer solution of pH 7.2 [% DMSO: % HBSS = 0.01: 99.99; $c = 2.5 \times 10^{-5}$ M] at 298 K are shown in Fig. 4. The excitation spectrum was recorded by monitoring the $^5D_0 \rightarrow {}^7F_2$ (612 nm) transition of the Eu^{3+} ion. The excitation spectrum displays a broad band between 280 and 425 nm, which can be designated to the π–π* electronic transition of the β-diketonate ligand. The absence of any absorption bands due to the f–f transitions of the Eu^{3+} ion clearly attests that luminescence sensitization *via* the excitation of the ligand is effective. The room temperature (298 K) emission spectrum of the europium complex was recorded in a buffer solution of pH = 7.2 by excitation at 405 nm and the pertinent results are depicted in Fig. 4. The emission bands of the europium complex are observed at 580, 593, 612, 652 and 697 nm, and are attributed to the f–f transitions of $^5D_0 \rightarrow {}^7F_J$ with J = 0, 1, 2, 3 and 4, respectively.[22] The transition of the highest intensity is dominated by the hypersensitive $^5D_0 \rightarrow {}^7F_2$ transition which occurs around 612 nm, indicating that Eu^{3+} is not located in a site with inversion center symmetry. Moreover, the presence of only one sharp peak in the region of the $^5D_0 \rightarrow {}^7F_0$ transition at 580 nm suggests the existence of a single chemical environment around Eu^{3+}. No broad emission band resulting from the organic ligand molecule in the blue region can be observed, which indicates that the ligand transfers the absorbed energy effectively to the emitting level of the metal ion.

The luminescence lifetime of the designed europium complex was measured at room temperature from the luminescence decay profile by fitting with the monoexponential decay curve (Fig. 5) and the lifetime data are shown in Table 1. These data indicate the existence of a single chemical environment around Eu^{3+}. To gain a better understanding of the luminescence efficiency of the designed Eu^{3+} compound, it was appropriate to analyse the emission profile of the complex in terms of eqn (2),[4d,23]

$$\Phi_{overall} = \Phi_{sens} \times \Phi_{Ln} = \Phi_{sens} \times (\tau_{obs}/\tau_{rad}) \quad (2)$$

where $\Phi_{overall}$ and Φ_{Ln} represent the overall and intrinsic luminescence quantum yields of Eu^{3+}; Φ_{sens} represents the efficiency of the ligand-to-metal energy transfer, and τ_{obs} and τ_{rad} are the observed and the radiative lifetimes of Eu^{3+} ($^5D_0$). Due to the low absorption intensities of direct f–f excitation, the intrinsic luminescence quantum yields of Eu^{3+} could not

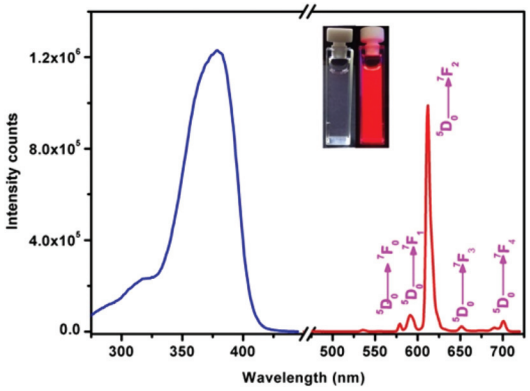

Fig. 4 Solution-state excitation and emission spectra $Eu(pfphOCH_3IN)_3$ (DDXPO) in a buffer solution of pH 7.2 [% DMSO : % HBSS = 0.01 : 99.99; $c = 2.5 \times 10^{-5}$ M] at 298 K, emission monitored at around 612 nm (λ_{ex} = 405 nm). Inset: Photograph of complex **4** in buffer solution under day light and UV light with 365 nm excitation.

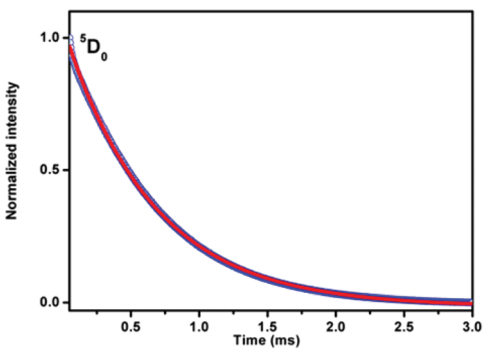

Fig. 5 The $^5D_0$ decay profile for complex **4** in a buffer solution of pH 7.2 [% DMSO : % HBSS = 0.01 : 99.99; $c = 2.5 \times 10^{-5}$ M] at 298 K, excited at 405 nm. The emission was monitored at 612 nm.

Table 1 Photophysical parameters, radiative lifetime (τ_{rad}), $^5D_0$ lifetime (τ_{obs}), intrinsic quantum yield (Φ_{Ln}) energy transfer efficiency (Φ_{sens}), and overall quantum yield ($\Phi_{overall}$) for selected europium complexes

Complex	τ_{rad} (ms)	τ_{obs} (ms)	Φ_{Ln} (%)	Φ_{sens} (%)	$\Phi_{overall}$ (%)	λ_{exc} (nm)
Eu(pfphOCH$_3$IN)$_3$(DDXPO)	1.7	0.398	23	~100	25 ± 3	405
[a][EuL^1]$^{3-}$ 1*b*	—	1.050	—	—	26	355
[a][EuL^3]$^{3+}$ 1*b*	—	1.030	—	—	17	355
[b][EuL^9]$^{3-}$ 11*b*	—	1.040	—	—	26	355
[c][Eu$_2$(L^{C2})$_3$]^{10c}	6.9	2.430	36	58	21	405
[c][Eu$_2$(L^{C5})$_3$]^{10c}	6.7	3.300	35	26	8.9	405

[a] In water at pH 6.5 ref. 1*b*. [b] In water at pH 6.5 ref. 11*b*. [c] In tris-HCl buffer at pH 7.4 ref. 10*c*.

be determined experimentally. Hence, the radiative lifetime of Eu^{3+} ($^5D_0$) has been calculated from eqn (3),

$$1/\tau_{rad} = A_{MD,0} \times n^3 \times (I_{tot}/I_{MD}) \quad (3)$$

where n represents the refractive index (1.33) of the medium. $A_{MD,0}$ is the spontaneous emission probability for the $^5D_0 \rightarrow {}^7F_1$ transition *in vacuo* (14.65 s^{-1}), and I_{tot}/I_{MD} signifies the ratio of the total integrated intensity of the corrected Eu^{3+} emission spectrum to the integrated intensity of the magnetic dipole $^5D_0 \rightarrow {}^7F_1$ transition. The intrinsic quantum yield for the synthesized Eu^{3+}–β-diketonate complex has been calculated from the ratio τ_{obs}/τ_{rad} and the pertinent value is tabulated in Table 1. The radiative lifetime (τ_{rad}), $^5D_0$ lifetime (τ_{obs}), energy transfer efficiency (Φ_{sens}), and overall quantum yield ($\Phi_{overall}$) for the developed europium complex are also presented in Table 1. Most importantly, the current results disclose that the newly developed europium complex exhibits impressive quantum yield ($\Phi_{overall}$ = 25%) in the solution state under biological pH conditions, which is found to be the highest so far reported for visible light excited europium complex systems (Table 1).[1b,10c,11b]

The photostability of the Eu(pfpHOCH$_3$IN)$_3$(DDXPO) complex

The photostability of complex **4** was inspected by means of measuring the photoluminescence intensity at 612 nm in a buffer solution of pH 7.2 [% DMSO : % HBSS = 0.01 : 99.99; c = 2.5 × 10^{-5} M] at 298 K, as a function of irradiation time. λ_{exc} = 405 nm, for 5 h and the results are given in Fig. 6. These results validated that the emission intensity of the complex at 612 nm remains approximately the same after 5 h of continuous irradiation. This indicates the stability of the Eu^{3+} complex towards photoirradiation.

Cell-imaging properties of Eu(pfphOCH$_3$IN)$_3$(DDXPO)

To evaluate the cytotoxic effects, the cytotoxicity of the developed europium complex was evaluated using the methyl thiazolyl tetrazolium (MTT) assay in mouse pre-adipocyte cell lines (3T3L1) and the results are depicted in Fig. 7.

Upon incubation with different concentrations of the europium complex from 0.0 to 125 μM for 24 h, no significant differences in the cell proliferation of the cells were observed. The cellular viability was greater than 99%. It is noted that when the concentration of the complex increased to 125 μM, the cell viability still remained above 90%. The results of the MTT assay clearly demonstrate that the europium compound is non-cytotoxic.

In the subsequent experiments, the 3T3L1 cells were grown on plastic-bottomed cell culture μ-dishes and incubated with a solution of the europium complex in DMEM (0.5–50 μM) for 24 h at 37 °C. The luminescence images recorded with an excitation wavelength of 405 nm are shown in Fig. 8. Bright spots start to appear in the cytoplasm of the cells for an incubation concentration as low as 0.5 μM. The results demonstrated that the luminescence intensity of the cells increases with an increase in the concentration of the europium complex (Fig. 9). The uptake of the europium compound at an

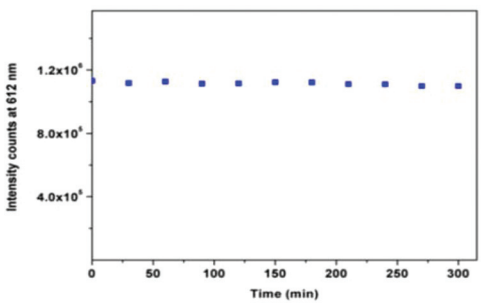

Fig. 6 Photoluminescence intensity of complex Eu(pfphOCH$_3$IN)$_3$ (DDXPO) at 612 nm in a buffer solution of pH 7.2 [% DMSO : % HBSS = 0.01 : 99.99; c = 2.5 × 10^{-5} M] at 298 K, as a function of irradiation time. λ_{exc} = 405 nm.

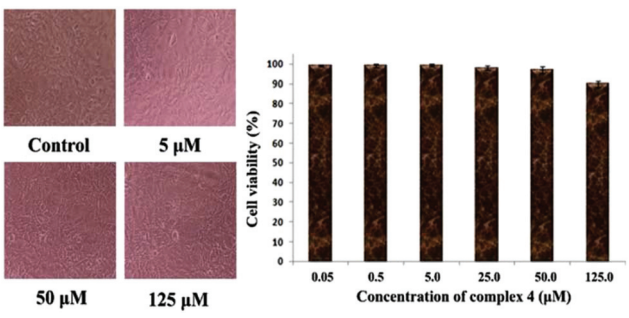

Fig. 7 The change in cell viability after incubating 3T3L1 cells with different concentrations of Eu(pfphOCH$_3$IN)$_3$(DDXPO) (representative images shown) and the graphical representation showing cell viability assessed by MTT assay.

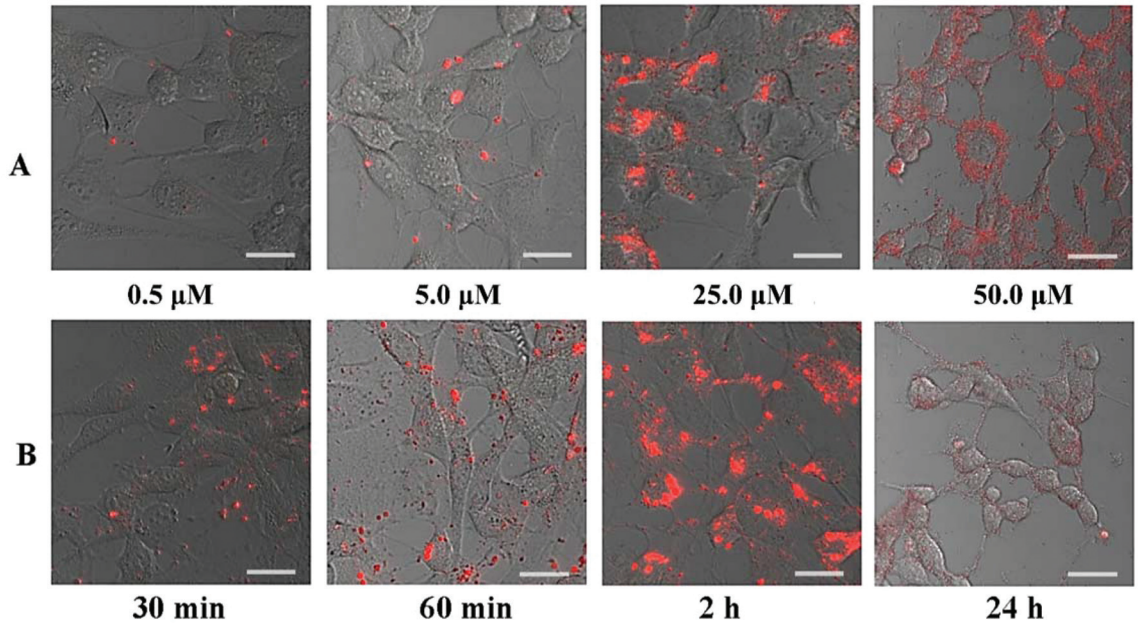

Fig. 8 Eu(pfphOCH$_3$IN)$_3$(DDXPO) was incubated with 3T3L1 cells at different concentrations and time intervals. Lane A shows the luminescence emitted by the compound at different concentrations after 24 h incubation. Lane B is the images of luminescence from cells after an incubation of 25 μM Eu(pfphOCH$_3$IN)$_3$(DDXPO) at different time intervals. Scale bars: 10 μm.

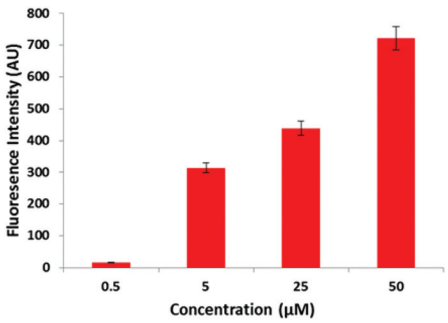

Fig. 9 The intensity of the complex Eu(pfphOCH$_3$IN)$_3$(DDXPO) in the cells *versus* the incubation concentration of complex **4**.

incubation concentration of 25 μM was investigated *versus* time and the emission from the europium compound can be detected after 30 min and the results are depicted in Fig. 8.

Another interesting feature of the developed europium complex is its chemical stability at ambient temperatures and it requires less incubation time (2 h) compared to the commercial lysosome tracker, CellLight® Lysosome-GFP (16 h).

In order to understand the sub-cellular localization of the europium complex, a lysosome targeted green fluorescent protein (CellLight® Lysosome-GFP, BacMam 2.0) was used for the co-localization experiments. The 3T3L1 cells were first loaded with the lysosome tracker and incubated at 37 °C for 16 h. Subsequently, the cells loaded with the Lysosome-GFP were incubated with 25 μM of the europium complex for 2 h and the results were examined under a confocal microscope using an appropriate filter. The green fluorescent signals representing the lysosome tracker in the 3T3L1 cell line were examined by excitation at 488 nm and emission monitoring at 510 nm (Fig. 10b). On the other hand, red luminescence signals of the europium complex were obtained at a 405 nm excitation and by emission monitoring at 612 nm (Fig. 10c). The extensive overlapping with Lyso-Tracker Green indicated that the lysosome is probably the main site of the europium

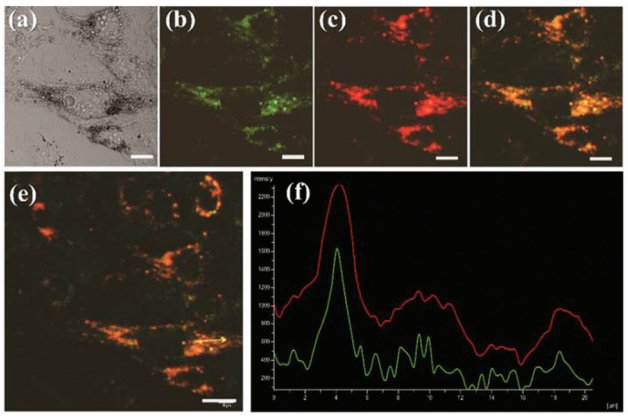

Fig. 10 Co-localization imaging of the 3T3L1 cells incubated with complex **4** and lysosome-GFP. (a) The bright field image; (b) luminescence image of GFP tagged lysosomal protein d(Ex. 488/Em. 520); (c) luminescence image of Eu(pfphOCH$_3$IN)$_3$(DDXPO) (Ex. 405/Em. 612); (d) merged image of (b) and (c); (e) representative image from which the luminescence emission intensity of both (GFP & complex **4**) is measured (region showed along the arrow line) and (f) the graphical representation of the luminescence intensity of lysosome-GFP (green) and Eu(pfphOCH$_3$IN)$_3$(DDXPO) (red). Scale bars: 10 μm.

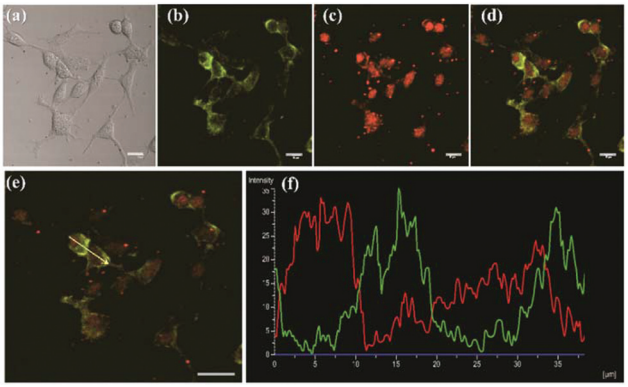

Fig. 11 Co-localization imaging of the 3T3L1 cells incubated with complex **4** and Mito-GFP. (a) The bright field image; (b) luminescence image of GFP tagged mitochondrial protein (Ex. 488/Em. 520); (c) luminescence image of Eu(pfphOCH$_3$IN)$_3$(DDXPO) (Ex. 405/Em. 612); (d) the merged image of (b) and (c); (e) representative image from which the luminescence emission intensity of both (GFP & complex **4**) is measured (region showed along the arrow line) and (f) the graphical representation of the luminescence intensity of GFP (green) and Eu(pfphOCH$_3$IN)$_3$(DDXPO) (red). Scale bars: 10 μm.

complex accumulation (Fig. 10d). Furthermore, the merged image of channel 1 and channel 2 (Fig. 10e) showed the vast overlap between the red luminescence of the europium complex and the green luminescence of Lyso-Tracker Green in the cells. Moreover, the luminescence intensity profile of the europium complex and Lysosome-GFP Green in the region of interest across the 3T3L1 cells is in very close synchrony (Fig. 10f). The colocalization coefficient, *A*, was calculated by using Pearson's method to evaluate the colocalization of complex **4** relative to the commercial probe (Lysosome-GFP).[24] The results demonstrate the colocalization of europium complex **4** with Lysosome-GFP with $A = 0.83$. All of these results demonstrated the specific-localization of the developed europium complex in the lysosome of the cells, suggesting that the europium complex could truly be used as a probe for tracking the intracellular lysosome.

To further figure out the europium complex localization, the mitochondria targeted green fluorescent protein (CellLight mito-GFP, BacMam 2.0) was also examined to find whether the europium complex can be localised within the other subcellular domains (Fig. 11). It can be clearly observed from Fig. 11e and f that no co-localization of the europium complex with mitochondria tracker green occurred. Moreover, the colocalization coefficient (*A*) of complex **4** relative to the commercial probe (mito-GFP) is found to be lower ($A = 0.46$).[24]

Conclusions

In summary, a unique bright luminescent europium coordination compound with excellent biocompatibility has been developed that serves as a selective bioprobe for particular organelles within the cells. The designed europium compound showed distinct advantages of visible-light excitation wavelength and remarkable quantum yield and luminescence lifetime values, which enabled it to be successfully utilized for visible-light excited luminescence cell imaging applications. Strikingly, the europium luminescent compound showed no observed cytotoxicity, high photostability and remains localized in the lysosomes of the 3T3L1 cells. The results demonstrated in the current study highlight that the developed luminescent europium compound has potential applications in live-cell imaging.

Acknowledgements

One of the authors T. M. George acknowledges financial support from the UGC, New Delhi for the award of a Senior Research Fellowship.

References

1 (*a*) M. C. Heffern, L. M. Matosziuk and T. J. Meade, *Chem. Rev.*, 2014, **114**, 4496–4539; (*b*) S. J. Butler, L. Lamarque, R. Pal and D. Parker, *Chem. Sci.*, 2014, **5**, 1750–1756; (*c*) M. L. P. Reddy, V. Divya and R. Pavithran, *Dalton Trans.*, 2013, **42**, 15249–15262; (*d*) L. Prodi, E. Rampazzo, F. Rastrelli, A. Speghini and N. Zaccheroni, *Chem. Soc. Rev.*, 2015, **44**, 4922–4952; (*e*) A. J. Amoroso and S. J. A. Pope, *Chem. Soc. Rev.*, 2015, **44**, 4723–4742; (*f*) J.-C. G. Bünzli, *Chem. Rev.*, 2010, **110**, 2729–2755; (*g*) M. Sy, A. Nonat, N. Hildebrandt and L. J. Charbonniere, *Chem. Commun.*, 2016, **52**, 5080–5095; (*h*) E. J. New, A. Congreve and D. Parker, *Chem. Sci.*, 2010, **1**, 111–118.

2 (*a*) J. Feng and H. Zhang, *Chem. Soc. Rev.*, 2013, **42**, 387–410; (*b*) M. L. P. Reddy and S. Sivakumar, *Dalton Trans.*, 2013, **42**, 2663–2678; (*c*) K. Binnemans, *Chem. Rev.*, 2009, **109**, 4283–4374; (*d*) C. Piguet and J.-C. G. Bünzli, *Chem. Soc. Rev.*, 1999, **28**, 347–358; (*e*) J.-C. G. Bünzli, A.-S. Chauvin, H. K. Kim, E. Deiters and S. V. Eliseeva, *Coord. Chem. Rev.*, 2010, **254**, 2623–2633; (*f*) A. de Bettencourt-Dias, P. S. Barber and S. Viswanathan, *Coord. Chem. Rev.*, 2014, **273–274**, 165–200; (*g*) Y. Ma and Y. Wang, *Coord. Chem. Rev.*, 2010, **254**, 972–990; (*h*) N. Sabbatini, M. Guardigli and J.-M. Lehn, *Coord. Chem. Rev.*, 1993, **123**, 201–228.

3 (*a*) X. Wang, H. Chang, J. Xie, B. Zhao, B. Liu, S. Xu, W. Pei, N. Ren, L. Huang and W. Huang, *Coord. Chem. Rev.*, 2014, **273–274**, 201–212; (*b*) J.-C. G. Bünzli, *J. Lumin.*, 2016, **170**, 866–878; (*c*) J.-C. G. Bünzli, *Interface Focus*, 2013, 3; (*d*) C. P. Montgomery, B. S. Murray, E. J. New, R. Pal and D. Parker, *Acc. Chem. Res.*, 2009, **42**, 925–937.

4 (*a*) S. V. Eliseeva and J.-C. G. Bünzli, *New J. Chem.*, 2011, **35**, 1165–1176; (*b*) L. Armelao, S. Quici, F. Barigelletti, G. Accorsi, G. Bottaro, M. Cavazzini and E. Tondello, *Coord. Chem. Rev.*, 2010, **254**, 487–505; (*c*) L. D. Carlos,

R. A. S. Ferreira, V. de Zea Bermudez, B. Julian-Lopez and P. Escribano, *Chem. Soc. Rev.*, 2011, **40**, 536–549; (*d*) J.-C. G. Bünzli and C. Piguet, *Chem. Soc. Rev.*, 2005, **34**, 1048–1077; (*e*) N. M. Shavaleev, S. V. Eliseeva, R. Scopelliti and J.-C. G. Bünzli, *Inorg. Chem.*, 2015, **54**, 9166–9173.

5 (*a*) S. Biju, N. Gopakumar, J.-C. G. Bünzli, R. Scopelliti, H. K. Kim and M. L. P. Reddy, *Inorg. Chem.*, 2013, **52**, 8750–8758; (*b*) K. Miyata, Y. Konno, T. Nakanishi, A. Kobayashi, M. Kato, K. Fushimi and Y. Hasegawa, *Angew. Chem., Int. Ed.*, 2013, **52**, 6413–6416; (*c*) J. Yuasa, T. Ohno, H. Tsumatori, R. Shiba, H. Kamikubo, M. Kataoka, Y. Hasegawa and T. Kawai, *Chem. Commun.*, 2013, **49**, 4604–4606; (*d*) V. Divya and M. L. P. Reddy, *J. Mater. Chem. C*, 2013, **1**, 160–170; (*e*) S. Sivakumar and M. L. P. Reddy, *J. Mater. Chem.*, 2012, **22**, 10852–10859; (*f*) S. Sivakumar, M. L. P. Reddy, A. H. Cowley and R. R. Butorac, *Inorg. Chem.*, 2011, **50**, 4882–4891; (*g*) T. M. George, S. Varughese and M. L. P. Reddy, *RSC Adv.*, 2016, **6**, 69509–69520; (*h*) V. Divya, S. Biju, R. L. Varma and M. L. P. Reddy, *J. Mater. Chem.*, 2010, **20**, 5220–5227; (*i*) A. R. Ramya, M. L. P. Reddy, A. H. Cowley and K. V. Vasudevan, *Inorg. Chem.*, 2010, **49**, 2407–2415; (*j*) A. R. Ramya, D. Sharma, S. Natarajan and M. L. P. Reddy, *Inorg. Chem.*, 2012, **51**, 8818–8826; (*k*) V. Divya, R. O. Freire and M. L. P. Reddy, *Dalton Trans.*, 2011, **40**, 3257–3268; (*l*) T. V. U. Gangan, S. Sreenadh and M. L. P. Reddy, *J. Photochem. Photobiol., A*, 2016, **328**, 171–181; (*m*) T. V. U. Gangan and M. L. P. Reddy, *Dalton Trans.*, 2015, **44**, 15924–15937.

6 (*a*) M. Soulié, F. Latzko, E. Bourrier, V. Placide, S. J. Butler, R. Pal, J. W. Walton, P. L. Baldeck, B. Le Guennic, C. Andraud, J. M. Zwier, L. Lamarque, D. Parker and O. Maury, *Chem. – Eur. J.*, 2014, **20**, 8636–8646; (*b*) J.-C. G. Bünzli and S. V. Eliseeva, *J. Rare Earths*, 2010, **28**, 824–842.

7 (*a*) F. J. Steemers, W. Verboom, D. N. Reinhoudt, E. B. van der Tol and J. W. Verhoeven, *J. Am. Chem. Soc.*, 1995, **117**, 9408–9414; (*b*) P. P. Lima, M. M. Nolasco, F. A. A. Paz, R. A. S. Ferreira, R. L. Longo, O. L. Malta and L. D. Carlos, *Chem. Mater.*, 2013, **25**, 586–598; (*c*) D. B. Ambili Raj, S. Biju and M. L. P. Reddy, *J. Mater. Chem.*, 2009, **19**, 7976–7983; (*d*) D. B. A. Raj, B. Francis, M. L. P. Reddy, R. R. Butorac, V. M. Lynch and A. H. Cowley, *Inorg. Chem.*, 2010, **49**, 9055–9063; (*e*) T. M. George, M. J. Sajan, N. Gopakumar and M. L. P. Reddy, *J. Photochem. Photobiol., A*, 2016, **317**, 88–99.

8 (*a*) J. Wu, G. Wang, D. Jin, J. Yuan, Y. Guan and J. Piper, *Chem. Commun.*, 2008, 365–367; (*b*) J. Wu, Z. Ye, G. Wang, D. Jin, J. Yuan, Y. Guan and J. Piper, *J. Mater. Chem.*, 2009, **19**, 1258–1264.

9 (*a*) D. Maurel, J. Kniazeff, G. Mathis, E. Trinquet, J.-P. Pin and H. Ansanay, *Anal. Biochem.*, 2004, **329**, 253–262; (*b*) J. M. Zwier, H. Bazin, L. Lamarque and G. Mathis, *Inorg. Chem.*, 2014, **53**, 1854–1866; (*c*) M. Rajendran, E. Yapici and L. W. Miller, *Inorg. Chem.*, 2014, **53**, 1839–1853; (*d*) S. Petoud, S. M. Cohen, J.-C. G. Bünzli and K. N. Raymond, *J. Am. Chem. Soc.*, 2003, **125**, 13324–13325; (*e*) J. Xu, T. M. Corneillie, E. G. Moore, G.-L. Law, N. G. Butlin and K. N. Raymond, *J. Am. Chem. Soc.*, 2011, **133**, 19900–19910; (*f*) B. Alpha, J.-M. Lehn and G. Mathis, *Angew. Chem., Int. Ed. Engl.*, 1987, **99**, 259–261.

10 (*a*) S. V. Eliseeva, G. Auböck, F. van Mourik, A. Cannizzo, B. Song, E. Deiters, A.-S. Chauvin, M. Chergui and J.-C. G. Bünzli, *Phys. Chem. B*, 2010, **114**, 2932–2937; (*b*) A. S. Chauvin, S. Comby, B. Song, C. D. Vandevyver, F. Thomas and J.-C. G. Bünzli, *Chem. – Eur. J.*, 2007, **13**, 9515–9526; (*c*) E. Deiters, B. Song, A.-S. Chauvin, C. D. B. Vandevyver, F. Gumy and J.-C. G. Bünzli, *Chem. – Eur. J.*, 2009, **15**, 885–900.

11 (*a*) Z. Dai, L. Tian, Y. Xiao, Z. Ye, R. Zhang and J. Yuan, *J. Mater. Chem. B*, 2013, **1**, 924–927; (*b*) S. J. Butler, M. Delbianco, L. Lamarque, B. K. McMahon, E. R. Neil, R. Pal, D. Parker, J. W. Walton and J. M. Zwier, *Dalton Trans.*, 2015, **44**, 4791–4803; (*c*) M. Li and P. R. Selvin, *J. Am. Chem. Soc.*, 1995, **117**, 8132–8138; (*d*) P. Kadjane, M. Starck, F. Camerel, D. Hill, N. Hildebrandt, R. Ziessel and L. J. Charbonnière, *Inorg. Chem.*, 2009, **48**, 4601–4603; (*e*) M. Starck, P. Kadjane, E. Bois, B. Darbouret, A. Incamps, R. Ziessel and L. J. Charbonnière, *Chem. – Eur. J.*, 2011, **17**, 9164–9179.

12 (*a*) N. N. Katia, A. Lecointre, M. Regueiro-Figueroa, C. Platas-Iglesias and L. J. Charbonnière, *Inorg. Chem.*, 2011, **50**, 1689–1697; (*b*) S. Mizukami, K. Tonai, M. Kaneko and K. Kikuchi, *J. Am. Chem. Soc.*, 2008, **130**, 14376–14377; (*c*) G. Piszczek, B. P. Maliwal, I. Gryczynski, J. Dattelbaum and J. R. Lakowicz, *J. Fluoresc.*, 2001, **11**, 101–107; (*d*) V.-M. Mukkala, C. Sund, M. Kwiatkowski, P. Pasanen, M. Högberg, J. Kankare and H. Takalo, *Helv. Chim. Acta*, 1992, **75**, 1621–1632.

13 (*a*) L. Tian, Z. Dai, Z. Ye, B. Song and J. Yuan, *Analyst*, 2014, **139**, 1162–1167; (*b*) V. Divya, V. Sankar, K. G. Raghu and M. L. P. Reddy, *Dalton Trans.*, 2013, **42**, 12317–12323; (*c*) J. Sun, B. Song, Z. Ye and J. Yuan, *Inorg. Chem.*, 2015, **54**, 11660–11668; (*d*) L. Zhang, L. Tian, Z. Ye, B. Song and J. Yuan, *Talanta*, 2013, **108**, 143–149; (*e*) G. L. Law, K. L. Wong, C. W. Y. Man, S. W. Tsao and W. T. Wong, *J. Biophotonics*, 2009, **2**, 718–724.

14 (*a*) S. J. Butler and D. Parker, *Chem. Soc. Rev.*, 2013, **42**, 1652–1666; (*b*) S. Pandya, J. Yu and D. Parker, *Dalton Trans.*, 2006, 2757–2766; (*c*) J. W. Walton, A. Bourdolle, S. J. Butler, M. Soulie, M. Delbianco, B. K. McMahon, R. Pal, H. Puschmann, J. M. Zwier, L. Lamarque, O. Maury, C. Andraud and D. Parker, *Chem. Commun.*, 2013, **49**, 1600–1602; (*d*) V. Placide, D. Pitrat, A. Grichine, A. Duperray, C. Andraud and O. Maury, *Tetrahedron Lett.*, 2014, **55**, 1357–1361.

15 M. Starck, R. Pal and D. Parker, *Chem. – Eur. J.*, 2016, **22**, 570–580.

16 O. V. Vieira, R. J. Botelho and S. Grinstein, *Biochem. J.*, 2002, **366**, 689–704.

17 (*a*) L. He, Y. Li, C.-P. Tan, R.-R. Ye, M.-H. Chen, J.-J. Cao, L.-N. Ji and Z.-W. Mao, *Chem. Sci.*, 2015, **6**, 5409–5418;

(*b*) L. He, S.-Y. Liao, C.-P. Tan, Y.-Y. Lu, C.-X. Xu, L.-N. Ji and Z.-W. Mao, *Chem. Commun.*, 2014, **50**, 5611–5614; (*c*) L. He, C.-P. Tan, R.-R. Ye, Y.-Z. Zhao, Y.-H. Liu, Q. Zhao, L.-N. Ji and Z.-W. Mao, *Angew. Chem., Int. Ed.*, 2014, **53**, 12137–12141; (*d*) X. Zhu, W. Lu, Y. Zhang, A. Reed, B. Newton, Z. Fan, H. Yu, P. C. Ray and R. Gao, *Chem. Commun.*, 2011, **47**, 10311–10313; (*e*) L. Murphy, A. Congreve, L.-O. Palsson and J. A. G. Williams, *Chem. Commun.*, 2010, **46**, 8743–8745; (*f*) Y.-M. Ho, N.-P. B. Au, K.-L. Wong, C. T.-L. Chan, W.-M. Kwok, G.-L. Law, K.-K. Tang, W.-Y. Wong, C.-H. E. Ma and M. H.-W. Lam, *Chem. Commun.*, 2014, **50**, 4161–4163.

18 (*a*) S. R. Meech and D. Phillips, *J. Photochem.*, 1983, **23**, 193–217; (*b*) D. F. Eaton, *Pure Appl. Chem.*, 1988, **60**, 1107–1114; (*c*) G. A. Crosby and J. N. Demas, *J. Phys. Chem.*, 1971, **75**, 991–1024.

19 J. K. Wilson, J. M. Sargent, A. W. Elgie, J. G. Hill and C. G. Taylor, *Br. J. Cancer*, 1990, **62**, 189–194.

20 (*a*) A. F. A. W. Woodward, A. R. Morales, J. Yu, A. F. Moore, A. D. Campiglia, E. V. Jucov, T. V. Timofeeva and K. D. Belfield, *Dalton Trans.*, 2014, **43**, 16639; (*b*) P. He, H. H. Wang, H. G. Yan, W. Hu, J. X. Shi and M. L. Gong, *Dalton Trans.*, 2010, **39**, 8919–8924.

21 (*a*) S. Sivakumar, M. L. P. Reddy, A. H. Cowley and K. V. Vasudevan, *Dalton Trans.*, 2010, **39**, 11690–11691; (*b*) A. R. Ramya, S. Varughese and M. L. P. Reddy, *Dalton Trans.*, 2014, **43**, 10940–10946.

22 S. Biju, Y. K. Eom, J.-C. G. Bünzli and H. K. Kim, *J. Mater. Chem. C*, 2013, **1**, 3454–3466.

23 (*a*) M. H. V. Werts, R. T. F. Jukes and J. W. Verhoeven, *Phys. Chem. Chem. Phys.*, 2002, **4**, 1542–1548; (*b*) N. M. Shavaleev, S. V. Eliseeva, R. Scopelliti and J.-C. G. Bünzli, *Inorg. Chem.*, 2010, **49**, 3927–3936; (*c*) B. Francis, C. Heering, R. O. Freire, M. L. P. Reddy and C. Janiak, *RSC Adv.*, 2015, **5**, 90720–90730; (*d*) B. Francis, D. B. A. Raj and M. L. P. Reddy, *Dalton Trans.*, 2010, **39**, 8084–8092.

24 (*a*) X. Chen, Y. Bi, T. Wang, P. Li, X. Yan, S. Hou, C. E. Bammert, J. Ju, K. M. Gibson, W. J. Pavan and L. Bi, *Sci. Rep.*, 2015, **5**, 9004; (*b*) X. Wang, D. M. Nguyen, C. O. Yanez, L. Rodriguez, H.-Y. Ahn, M. V. Bondar and K. D. Belfield, *J. Am. Chem. Soc.*, 2010, **132**, 12237–12239.